JOURNAL OF GUIDANCE, CONTROL, AND DYNAMICS
Vol. 36, No. 2, March–April 2013

Engineering Notes

Multi-Objective Optimization for Multiphase Orbital Rendezvous Missions

Jin Zhang*
National University of Defense Technology, 410073 Changsha, People's Republic of China
and
Geoffrey Parks†
University of Cambridge, Cambridge, England CB2 1PZ, United Kingdom

DOI: 10.2514/1.57786

I. Introduction

IN SPACE rendezvous and docking missions, to achieve the desired docking condition, the chaser (i.e., the active spacecraft) must execute many complicated operations, such as orbital maneuvers, relative navigation, and station maintenance. To obtain a stable orbital profile, several station-keeping points are deployed on the rendezvous trajectory [1], and then the rendezvous process is divided into several phases. Fehse [2] identified the common considerations for each rendezvous phase, and the planning of the rendezvous mission is usually performed phase by phase.

The optimal orbital rendezvous problem has been the subject of extensive research. The design variables are usually the burn time and maneuver impulse [3]. The design objective could be the velocity increment, time of flight [4], trajectory safety [5], or trajectory robustness [6]. The design constraints include the final relative position and velocity, minimum burn time interval, passive safety [7,8], and the working condition of navigation sensors [2]. However, only a small portion of previous studies have focused on the design of multiphase stable rendezvous profiles.

To improve the overall performance of a multiphase rendezvous mission, in addition to the parameters in each individual phase, the parameters at the interface between different phases should also be investigated. These interface parameters include the relative distances of station-keeping points as well as the keeping duration and the orbital transfer duration of each rendezvous phase. In a previous study by the first author [9], a multiphase orbital rendezvous mission was optimized using mixed-integer nonlinear programming. The objective in that study was a combination of the propellant consumption, the available sun power index, and a trajectory-robustness index. Nevertheless, that study had two obvious deficiencies. First, the various design objectives are combined by using weighting factors, which are difficult to determine in practice. Second, the optimization approach adopted obscures the relationships between the various objectives, and the characteristics of the multiphase orbital rendezvous problem are not clearly shown either.

A rendezvous mission with multiple objectives is the focus of some deep space exploration missions [10,11]. However, in these studies, multiple objectives are usually combined into one integral objective by weighting factors. To obtain multiple Pareto-optimal solutions, rather than a single optimum for the integral objective, Luo et al. employed multi-objective optimization algorithms to optimize linearized impulse rendezvous trajectories [12], two-body impulse rendezvous trajectories [13], and perturbed impulse rendezvous trajectories [14]. The main limitation of Luo et al.'s research is that it is only valid for single-phase rendezvous missions. Vasile and Zuiani proposed an agent-based memetic multi-objective optimization algorithm and applied it to two-body trajectory design and multi-gravity-assist trajectory design without engineering constraints [15].

The purpose of this paper is to propose and demonstrate a multi-objective optimization method for multiphase rendezvous missions, with consideration of engineering constraints. First, a multiphase rendezvous mission scenario is presented, and then the multi-objective multiphase rendezvous optimization model is built. After that, this model is solved by a multi-objective genetic algorithm (MOGA). Finally, a representative numerical problem is used to validate the proposed method, to reveal the relationships between different design objectives, and to analyze the characteristics of the multiphase orbital rendezvous missions.

II. Multiphase Rendezvous Mission

In the orbital rendezvous research domain, the chaser's movement is usually described in the target-centered orbital coordinate system o-xyz, which is defined as follows [2]:

The z axis, also called R-bar, is along the position vector from the target spacecraft to the earth.

The y axis, also called H-bar, is in the opposite direction to the orbit normal.

The x axis, also called V-bar, is in the direction of the velocity and completes the right-handed system.

As shown in Fig. 1, several station-keeping points are deployed on the V-bar of the target. The chaser first keeps station at K_0, either due to an emergency departure or due to a re-rendezvous experiment. Then the chaser transfers from K_0 to K_N using N sets of maneuvers, with keeping station at $K_i (i = 1, \ldots, N)$. Thus, the rendezvous mission is divided into N phases. The maneuvers are controlled onboard, using the information obtained by two optical navigation sensors, switching sensor at a point S. During the final approach from K_N to the docking point, the chaser's position, velocity, attitude, and angular rate are controlled simultaneously in a closed-loop mode. The details of the main operations in this multiphase rendezvous mission are described as follows.

A. Station Maintenance

At the station-keeping points, the relative velocity must be sufficiently small that the relative position changes slowly. To obtain a stable orbital profile, the mission is checked both onboard and on-ground when the chaser executes station-keeping operations.

Let $r_i = |x_{K_i}|$ be the relative distance of K_i from the target center O, and let dur_i be the station-keeping duration at K_i. Both r_i and dur_i are phase-connecting parameters between the ith and $(i-1)$th phases; r_i affects the shape of the relative trajectory and propellant consumption. By adjusting dur_i, the sun-illumination window and the communication window can be synchronized [2]. Nowadays, thanks to the widespread use of tracking and data relay satellite systems (TDRSS), it is easy to build a communication chain between rendezvous spacecraft and the mission control center through the

Received 31 January 2012; revision received 25 June 2012; accepted for publication 13 August 2012; published online 12 February 2013.

*Ph.D. Candidate, College of Aerospace Science and Engineering; zhangjinxy@yahoo.com.cn (Corresponding Author).

†Senior Lecturer, Department of Engineering; gtp@eng.cam.ac.uk.

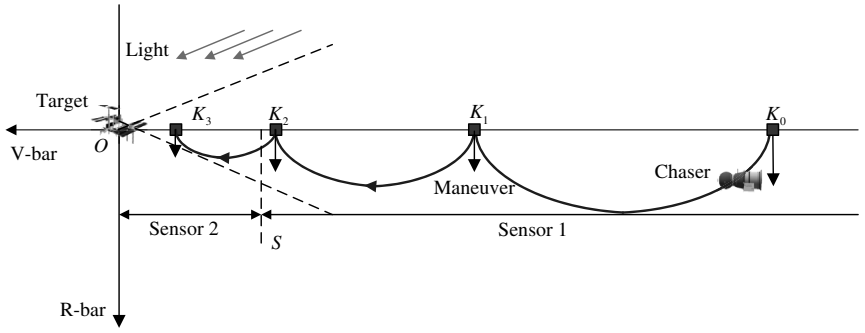

Fig. 1 Multiphase rendezvous mission profile.

TDRSS, and therefore dur_i is mainly used to synchronize the sun-illumination window.

B. Orbital Transfer

In this research, only coplanar relative motion is considered. The chaser's orbital transfer from K_{i-1} to K_i is calculated onboard on the basis of the well known Clohessy–Wiltshire equations [2]:

$$\begin{cases} \ddot{x} - 2\omega\dot{z} = a_x \\ \ddot{z} + 2\omega\dot{x} - 3\omega^2 z = a_z \end{cases} \tag{1}$$

where ω is the mean orbital angular rate of the target, and a_x and a_z are chaser's thrust-acceleration components.

Let t_i^- and t_i^+ be the chaser's arrival and departure times at K_i, respectively, and let Δt_i be the transfer time from K_{i-1} to K_i. Thus,

$$t_i^- = t_{i-1}^+ + \Delta t_i \tag{2}$$

$$t_i^+ = t_i^- + \text{dur}_i \tag{3}$$

It is assumed that only two maneuvers are involved within each rendezvous phase, and these are executed at t_{i-1}^+ and t_i^-, respectively. Based on Eq. (2), the impulsive orbital transfer from K_{i-1} to K_i can be expressed as follows:

$$\mathbf{X}(t_i^-) = \mathbf{\Phi}(t_i^-, t_{i-1}^+)\mathbf{X}(t_{i-1}^+) + \mathbf{\Phi}_v(t_i^-, t_{i-1}^+)\Delta\mathbf{v}_{i-1}^+ + \mathbf{\Phi}_v(t_i^-, t_i^-)\Delta\mathbf{v}_i^- \tag{4}$$

where

$$\mathbf{X} = \begin{bmatrix} \mathbf{r} \\ \mathbf{v} \end{bmatrix}, \qquad \mathbf{r} = \begin{bmatrix} x \\ z \end{bmatrix}, \qquad \mathbf{v} = \begin{bmatrix} \dot{x} \\ \dot{z} \end{bmatrix}$$

$$s = \sin[\omega(\tau_2 - \tau_1)], \qquad c = \cos[\omega(\tau_2 - \tau_1)]$$

$$\mathbf{\Phi}(\tau_2, \tau_1) = \begin{bmatrix} \mathbf{\Phi}_{rr}(\tau_2, \tau_1) & \mathbf{\Phi}_{rv}(\tau_2, \tau_1) \\ \mathbf{\Phi}_{vr}(\tau_2, \tau_1) & \mathbf{\Phi}_{vv}(\tau_2, \tau_1) \end{bmatrix}$$

$$\mathbf{\Phi}_v(\tau_2, \tau_1) = \begin{bmatrix} \mathbf{\Phi}_{rv}(\tau_2, \tau_1) \\ \mathbf{\Phi}_{vv}(\tau_2, \tau_1) \end{bmatrix}$$

$$\mathbf{\Phi}_{rr}(\tau_2, \tau_1) = \begin{bmatrix} 1 & 6[\omega(\tau_2 - \tau_1) - s] \\ 0 & 4 - 3c \end{bmatrix}$$

$$\mathbf{\Phi}_{rv}(\tau_2, \tau_1) = \begin{bmatrix} \frac{4s - 3\omega(\tau_2 - \tau_1)}{\omega} & \frac{2(\tau_2 - \tau_1)}{\omega} \\ \frac{2(c-1)}{\omega} & \frac{s}{\omega} \end{bmatrix}$$

$$\mathbf{\Phi}_{vr}(\tau_2, \tau_1) = \begin{bmatrix} 0 & 6\omega(1-c) \\ 0 & 3\omega s \end{bmatrix}$$

and

$$\mathbf{\Phi}_{vv}(\tau_2, \tau_1) = \begin{bmatrix} 4c - 3 & 2s \\ -2s & c \end{bmatrix}$$

Analytical solutions of Eq. (4) are given by Eqs. (5, 6):

$$\Delta\mathbf{v}_{i-1}^+ = \mathbf{\Phi}_{rv}^{-1}(t_i^-, t_{i-1}^+)[\mathbf{r}(t_i^-) - \mathbf{\Phi}_{rr}(t_i^-, t_{i-1}^+)\mathbf{r}(t_{i-1}^+) - \mathbf{\Phi}_{rv}(t_i^-, t_{i-1}^+)\mathbf{v}(t_{i-1}^+)] \tag{5}$$

$$\Delta\mathbf{v}_i^- = \mathbf{v}(t_i^-) - \mathbf{\Phi}_{vr}(t_i^-, t_{i-1}^+)\mathbf{r}(t_{i-1}^+) - \mathbf{\Phi}_{vv}(t_i^-, t_{i-1}^+)\mathbf{v}(t_{i-1}^+) - \mathbf{\Phi}_{vv}(t_i^-, t_{i-1}^+)\Delta\mathbf{v}_{i-1}^+ \tag{6}$$

The orbital transfer described previously is a nominal case. However, the effect of orbital errors needs to be considered. Different orbital errors can affect a rendezvous mission in the process of navigating, targeting, and burning. Targeting errors are mainly caused by the linear dynamic model, but their effects decrease as the chaser approaches the target. Therefore, navigating and burning errors are the main errors considered in this paper. The linear covariance method is used to propagate errors [16], and the interaction between the errors affecting the rendezvous mission at different times is ignored.

Let $\delta\mathbf{X}_{i-1}^+$ and $\delta\Delta\mathbf{v}_{i-1}^+$ be the navigation and burning errors at t_{i-1}^+, respectively, and let $\delta\mathbf{X}_i^-$ and $\delta\Delta\mathbf{v}_i^-$ be the navigation and burning errors at t_i^-, respectively.

Taking into account the corrective ability of each maneuver's retargeting, $\mathbf{r}(t_i^-)$ is mainly affected by $\delta\mathbf{X}_{i-1}^+$ and $\delta\Delta\mathbf{v}_{i-1}^+$, while $\mathbf{v}(t_i^-)$ is mainly affected by $\delta\mathbf{X}_i^-$ and $\delta\Delta\mathbf{v}_i^-$. Error-coupling effects, which appear as the off-diagonal elements of the covariance matrix, are neglected here. Error-coupling effects are significant only when the mission time is very long or the relative distance is large. The mission time of each rendezvous phase in this study is less than four orbital periods, and the relative distance is less than 5 km. Thus, it seems reasonable to assume that the coupling effect of errors is negligible. Therefore, the covariance matrix at the end of each rendezvous phase is given by

$$\begin{aligned} \mathbf{C}_{i-} = {} & \mathbf{E}_1[\mathbf{\Phi}(t_i^-, t_{i-1}^+)\mathbf{C}_{\delta\mathbf{X}_{i-1}^+}\mathbf{\Phi}(t_i^-, t_{i-1}^+)^T \\ & + \mathbf{\Phi}_v(t_i^-, t_{i-1}^+)\mathbf{C}_{\delta\Delta\mathbf{v}_{i-1}^+}\mathbf{\Phi}_v(t_i^-, t_{i-1}^+)^T] \\ & + \mathbf{E}_2[\mathbf{\Phi}(t_i^-, t_i^-)\mathbf{C}_{\delta\mathbf{X}_i^-}\mathbf{\Phi}(t_i^-, t_i^-)^T \\ & + \mathbf{\Phi}_v(t_i^-, t_i^-)\mathbf{C}_{\delta\Delta\mathbf{v}_i^-}\mathbf{\Phi}_v(t_i^-, t_i^-)^T] \end{aligned} \tag{7}$$

where $\mathbf{E}_1 = \text{diag}(1, 1, 0, 0)$, $\mathbf{E}_2 = \text{diag}(0, 0, 1, 1)$, and diag denotes a diagonal matrix; $\mathbf{C}_{\delta\mathbf{X}_{i-1}^+}$ and $\mathbf{C}_{\delta\mathbf{X}_i^-}$ are the navigation error covariance matrices at t_{i-1}^+ and t_i^-, respectively; and $\mathbf{C}_{\delta\Delta\mathbf{v}_{i-1}^+}$ and $\mathbf{C}_{\delta\Delta\mathbf{v}_i^-}$ are the maneuver error covariance matrices at t_{i-1}^+ and t_i^-, respectively.

$\sigma_x^2(t_i^-)$, $\sigma_z^2(t_i^-)$, $\sigma_{v_x}^2(t_i^-)$, and $\sigma_{v_z}^2(t_i^-)$ (i.e., the variances of trajectory dispersions at t_i^-) are the diagonal elements of the matrix $\mathbf{C}_{i-}$. The variance of the relative position dispersion is defined as

$$\sigma_r^2(t_i^-) = \sigma_x^2(t_i^-) + \sigma_z^2(t_i^-) \tag{8}$$

and the variance of the relative velocity dispersion is given by

$$\sigma_v^2(t_i^-) = \sigma_{v_x}^2(t_i^-) + \sigma_{v_z}^2(t_i^-) \tag{9}$$

$\sigma_r^2(t_i^-)$ and $\sigma_v^2(t_i^-)$ represent the trajectory robustness.

C. Relative Navigation

To obtain high navigation precision, two optical relative navigation sensors are used according to their different performance at different relative distances. As the chaser approaches the target, the working sensor will be switched from sensor 1 to sensor 2 at the point S with a relative distance of r_S. The optical sensors could be a lidar, charge-coupled device, or TV camera. During eclipse, some cooperative lighting drones on the target spacecraft would help the work of optical sensors.

That the target never appears out of the chaser's field of view is a basic working requirement of optical navigation sensors. As shown in Fig. 2, the chaser is assumed to hold an Earth-oriented attitude, and the field-of-view requirement is given by

$$\arctan\left[\left|\frac{z(t)}{x(t)}\right|\right] \le \frac{\mathrm{FOV}_{s_i 0}}{2} \left(t \in [t_{i-1}^+, t_i^-]\right) \tag{10}$$

where $s_i = 1$ or 2 identifies the serial number of the working sensor in the ith rendezvous phase, and $\mathrm{FOV}_{s_i 0}$ is the cone angle of the working sensor's field of view.

Another working requirement of optical navigation sensors relates to sun illumination. As shown in Fig. 3, in the orbital day, light from the sun may disturb the sensor when the sun appears directly in the sensor's field of view. In Fig. 3, FOV_0 is the cone angle of the sensor's field of view and α is the sun's line-of-sight angle in the sensor's view. Thus, the sun-illumination requirement during each rendezvous phase is given by

$$\alpha_i(t) \ge \frac{\mathrm{FOV}_{s_i 0}}{2} \left(t \in [t_{i-1}^+, t_i^-] \cap \mathbf{D}\right) \tag{11}$$

where $\mathbf{D}$ represents the time interval set of orbital days, and $\alpha_i(t)$ is calculated on the basis of the target's trajectory and the sun's position:

$$\begin{aligned}\alpha_i(t) = \arccos\{&\cos[\mathrm{inc}(t)]\cos[\varepsilon(t)]\cos[u(t)]\cos[\Omega(t)]\sin[\lambda(t)] \\ &+ \cos[u(t)]\sin[\mathrm{inc}(t)]\sin[\varepsilon(t)]\sin[\lambda(t)] \\ &- \cos[\lambda(t)]\cos[\Omega(t)]\sin[u(t)] \\ &- \cos[\mathrm{inc}(t)]\cos[\lambda(t)]\cos[u(t)]\sin[\Omega(t)] \\ &- \cos[\varepsilon(t)]\sin[\lambda(t)]\sin[u(t)]\sin[\Omega(t)]\}\end{aligned} \tag{12}$$

where inc is the orbital inclination, Ω is the right ascension of ascending node (RAAN), and u is the argument of latitude; λ and ε are the ecliptic longitude and the obliquity of the ecliptic, respectively, and they represent the sun's position.

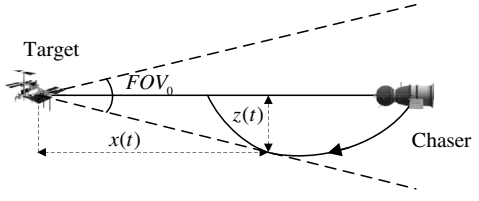

Fig. 2 Geometry of the field-of-view requirement.

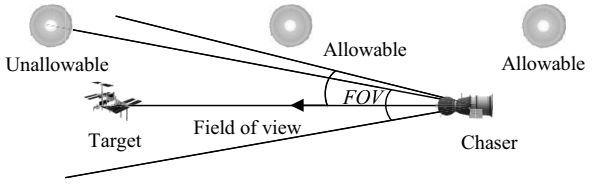

Fig. 3 Geometry of the sun-illumination requirement.

III. Optimization Model

This section presents the design variables, objective functions, and constraints of the multiphase rendezvous optimization problem and then gives a simple description of the MOGA.

A. Optimization Problem

The design variables include the relative distances and keeping duration of station-keeping points and the orbital transfer time of different rendezvous phases:

$$\mathbf{x} = [r_1, \ldots, r_{N-1}, \mathrm{dur}_0, \mathrm{dur}_1, \ldots, \mathrm{dur}_N, \Delta t_1, \ldots, \Delta t_N]^T \tag{13}$$

where dur_0 is the station-keeping duration at K_0 from the time when the chaser is able to start the multiphase rendezvous mission to the time when the chaser leaves K_0.

Three design objectives are involved. The first objective is the total velocity increment:

$$\min f_1 = \sum_{i=1}^{N} (|\Delta v_{x(i-1)}^+| + |\Delta v_{z(i-1)}^+| + |\Delta v_{xi}^-| + |\Delta v_{zi}^-|) \tag{14}$$

The total rendezvous time of flight is used as the second objective:

$$\min f_2 = \mathrm{dur}_0 + \Delta t_f + \sum_{i=1}^{N} (\mathrm{dur}_i + \Delta t_i) \tag{15}$$

where Δt_f is the time of the final approach, which is fixed in this study.

The third design objective is to maximize the trajectory robustness. This is expressed by minimizing the combined trajectory dispersion as given next:

$$\min f_3 = \sum_{i=1}^{N} \left[\frac{\sigma_r(t_i^-)}{r_i} + \frac{\sigma_v(t_i^-)}{\omega r_i}\right] \tag{16}$$

$2N + 1$ constraints in total need to be considered, including the trajectory field-of-view requirements and the sun-illumination requirements. The field-of-view requirements within different rendezvous phases are expressed as

Table 1 Search intervals of design variables

Phase number	r_i (m)	dur_i (s)	Δt_i (s)
1	(100, 5000)	$[120, 4T_0]$	$[600, 4T_0]$
2	(100, 5000)	$[120, 4T_0]$	$[600, 4T_0]$
3	(100, 5000)	$[120, 4T_0]$	$[600, 4T_0]$

Table 2 GA parameters

Parameter	Value
Population size	400
Maximum number of generations	200
Scale of tournament selection	3
Probability of crossover	0.8
Probability of mutation	0.3

Table 3 Single-objective optimal solutions

Number of phases	Design objective	Design variables for optimum	f_1(m/s)	f_2 (s)	f_3
$N = 3$	f_1	$(-1054.6$ m, -317.1 m, 0.0 s, 1993.8 s, 8904.5 s, 120.0 s, 1108.2 s, 600.0 s, 600.0 s$)^T$	15.415	13927	0.814
$N = 3$	f_2	$(-609.9$ m, -268.7 m, 0.0 s, 120.0 s, 120.0 s, 120.0 s, 600.0 s, 600.0 s, 600.0 s$)^T$	24.055	2760	1.066
$N = 3$	f_3	$(-1054.7$ m, -317.1 m, 0.0 s, 120.0 s, 136.7 s, 120.0 s, 850.8 s, 600.0 s, 600.0 s$)^T$	18.834	3028	0.800

$$g_i = \arctan\left[\left|\frac{z(t)}{x(t)}\right|\right] - \frac{\text{FOV}_{s_i 0}}{2} \le 0 \quad (t \in [t_{i-1}^+, t_i^-], i = 1, 2 \ldots, N) \tag{17}$$

The sun-illumination requirements within different rendezvous phases are given by

$$g_{i+N} = \frac{\text{FOV}_{s_i 0}}{2} - \alpha_i(t) \le 0 \quad (t \in [t_{i-1}^+, t_i^-] \cap \mathbf{D}, i = 1, 2 \ldots F, N) \tag{18}$$

The sun-illumination requirement during the final approach is expressed as

$$g_{2N+1} = \frac{\text{FOV}_{20}}{2} - \alpha_f(t) \le 0 \qquad (t \in [t_N^+, t_f] \cap \mathbf{D}) \tag{19}$$

B. Multi-Objective Genetic Algorithm

Generally, the objectives of a multi-objective optimization problem are at least partly conflicting, and optimization of one objective may result in deterioration of others. Therefore, a multi-objective optimization problem does not usually have a single optimal solution. Instead, the solution is a family of designs representing the tradeoffs between the competing objectives, known as the Pareto-optimal set.

A solution is not dominated if there is no other solution that is at least as good as the selected solution in all objectives and better in at least one objective. A nondominated set is a set among the solutions whose members do not dominate each other and are not dominated by any other solution. Then, the Pareto-optimal set is defined as the nondominated set of the problem's entire feasible solution space [17].

MOGA is a kind of genetic algorithm (GA) extended for multi-objective optimization. In GAs, the probability that a selected individual will be allowed to evolve is governed by its fitness value, which is usually a function of that individual's single-objective value and its constraint values. MOGA extends a GA's fitness assignment method so that it is applicable to multiple objectives [17].

There are many variants of MOGA reported in the literature, and a survey can be found in [17]. Among these variants, the nondominated sorting genetic algorithm (NSGA) developed by Srinivas and Deb has been widely applied [18]. NSGA-II [19] was developed from NSGA. It uses a fast nondominated sorting approach to identify the Pareto rank of each individual and employs a crowding distance assignment to estimate density. The NSGA-II algorithm thus transforms several objectives to a single fitness measure by creating a number of fronts sorted according to nondomination. The fitness of an individual is then its nondominated rank. NSGA-II uses a tournament selection scheme, within which the individual with the lower nondominated rank wins. If the solutions competing in the tournament come from the same front, the one with the largest crowding distance wins. Readers can refer to [19] for more information about NSGA-II.

The NSGA-II implementation adopted in this research is real-coded. An elitist strategy is also employed during the evolution of the population. This can help prevent the loss of good solutions once they have been found. Unlike the original version of NSGA-II, the arithmetical crossover operator and the nonuniform mutation operator are applied.

IV. Results

A. Problem Configuration

The mission initial time t_{00} in Gregorian universal coordinated time format is 13 March 2020 06:00:00.000, and $t_0^+ = t_{00} + \text{dur}_0$. The target runs in a two-day repeating-ground-track orbit, and its initial state (semimajor axis, eccentricity, inclination, RAAN, argument of periapsis, true anomaly) at t_{00} is

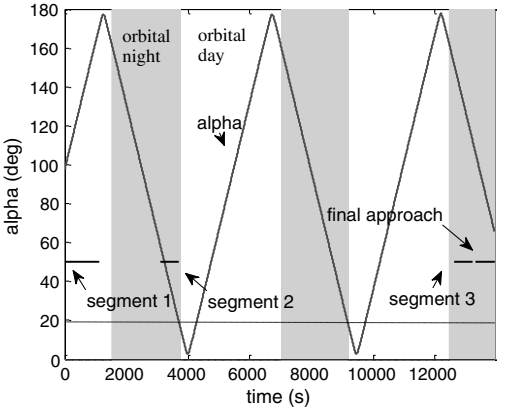

Fig. 5 Light condition of the minimum velocity increment solution for the three-phase mission.

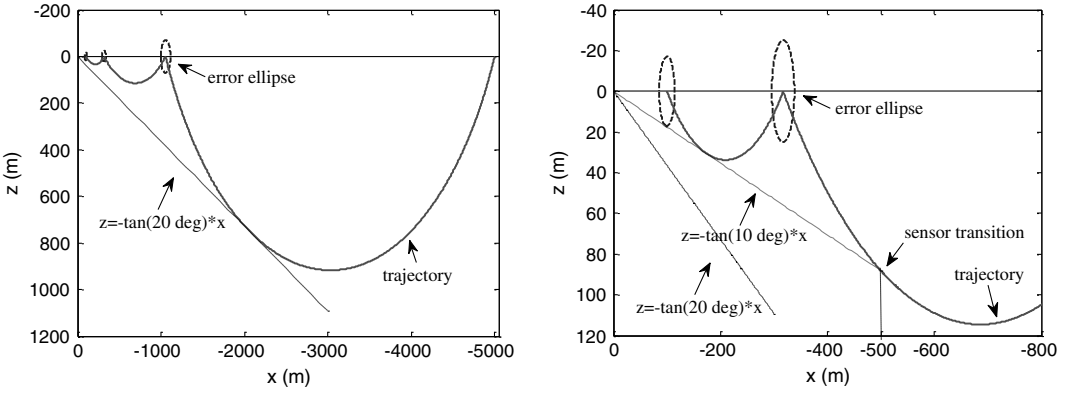

a) Complete trajectory **b) Close-up of the trajectory**

Fig. 4 Trajectory of the minimum velocity increment solution for the three-phase mission.

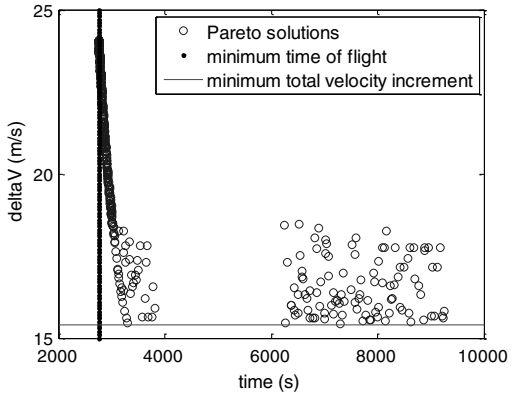

a) Total velocity increment vs. time of flight

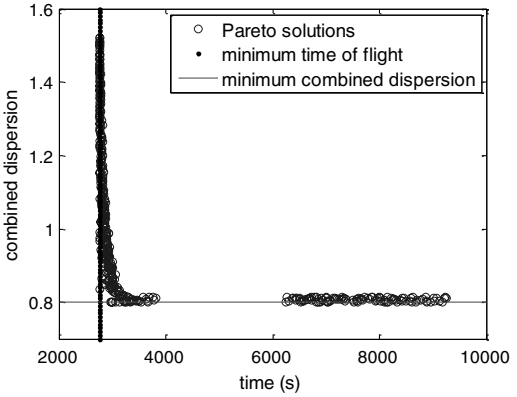

b) Combined dispersion vs. time of flight

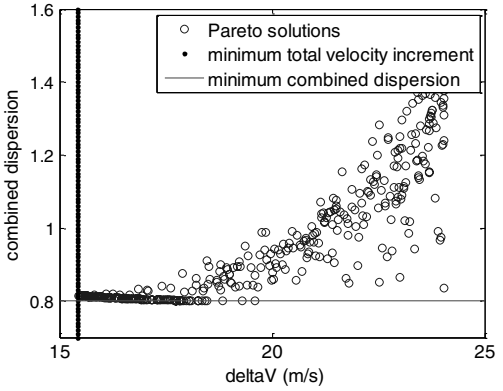

c) Combined dispersion vs. total velocity increment

Fig. 6 Three-objective Pareto-optimal fronts.

$$\mathbf{E}_{\text{tar0}} = [6714.2692\ \text{km}, 0, 42.4\ \text{deg}, 1.076063\ \text{deg}, 0\ \text{deg}, 0\ \text{deg}]$$

The target's trajectory is calculated before the optimization, using numerical trajectory integration only taking into account the J_2 term of the earth nonspherical perturbation. The orbital period T_0 is 5475.315 s, and the repeating period T is 169,441.345 s.

The multiphase rendezvous mission starts from K_0 with $x_{K_0} = -5000$ m, and the last station-keeping point is still behind the target with $x_{K_N} = -100$ m. $N = 3$, i.e., the rendezvous mission is divided into three phases.

The relative range of the sensor transition point is $r_S = 500$ m. The cone angles of the sensors' field of view are $\text{FOV}_{10} = 40$ deg and $\text{FOV}_{20} = 20$ deg. The covariance matrices of the navigation errors for two sensors are given as follows:

$$\text{diag}[(0.5\ \text{m} + 1.0 \times 10^{-3}\rho)^2, (0.5\ \text{m} + 1.0 \times 10^{-3}\rho)^2, (0.02\ \text{m/s})^2, (0.02\ \text{m/s})^2]$$

$$\text{diag}[(0.2\ \text{m} + 1.0 \times 10^{-3}\rho)^2, (0.2\ \text{m} + 1.0 \times 10^{-3}\rho)^2, (0.01\ \text{m/s})^2, (0.01\ \text{m/s})^2]$$

where ρ is the relative range of the point of measure. This error model represents the major characteristics of practical errors at a level of complexity suitable for use during mission planning. A more complicated exact error model would be needed for high-precision mission simulation.

The covariance matrices of burning errors for each orbit transfer are

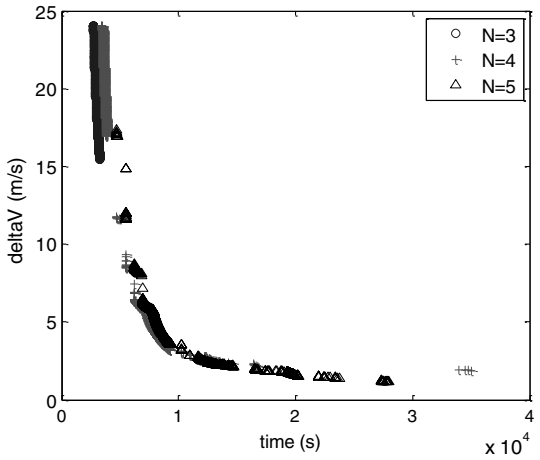

Fig. 7 Two-objective Pareto-optimal fronts comparison for different numbers of phases (total velocity increment vs time of flight).

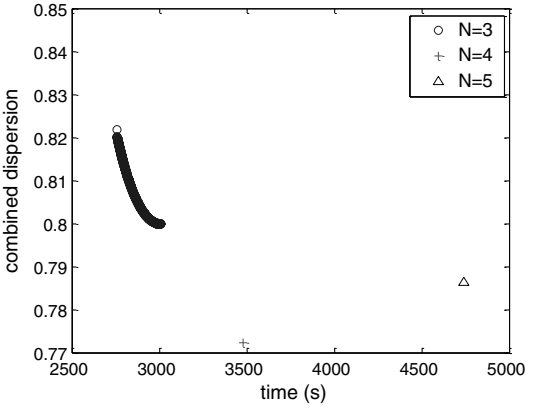

Fig. 8 Two-objective Pareto-optimal fronts comparison for different numbers of phases (combined dispersion vs time of flight).

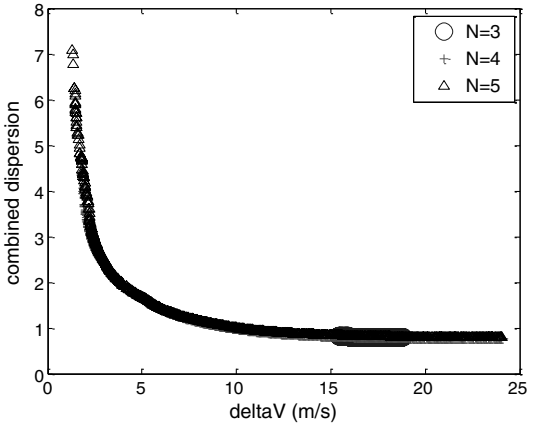

Fig. 9 Two-objective Pareto-optimal fronts comparison for different numbers of phases (combined dispersion vs total velocity increment).

$$\mathbf{C}_{\delta\Delta\mathbf{v}^+_{(i-1)}} = \mathrm{diag}[(0.02\ \mathrm{m/s} + 0.01\Delta v^+_{x(i-1)})^2, (0.02\ \mathrm{m/s} + 0.01\Delta v^+_{z(i-1)})^2]$$

$$\mathbf{C}_{\delta\Delta\mathbf{v}^-_i} = \mathrm{diag}[(0.02\ \mathrm{m/s} + 0.01\Delta v^-_{xi})^2, (0.02\ \mathrm{m/s} + 0.01\Delta v^-_{zi})^2]$$

The search interval of the station-keeping duration at K_0 is $\mathrm{dur}_0 \in [0, 4T_0]$, and the search intervals of the other design variables are provided in Table 1. The final approach time is $\Delta t_f = 600$ s. The GA parameters used are shown in Table 2. The sun's position is calculated based on the Jet Propulsion Laboratory ephemeris [20], and then the values of $\alpha(t)$ are obtained according to Eq. (12), using the information given by interpolating the sun's position data and the target trajectory already calculated.

B. Single-Objective Optimal Solutions

The single-objective optimal solutions are obtained using a single-objective version of the GA used, with the other algorithm parameter values being the same as those given in Table 2. These single-objective optima represent expected extremal solutions in a multi-objective optimization and help to show how the constraints under consideration are satisfied. The minimum total velocity increment solution, the minimum time of flight solution, and the most robust solution are presented in Table 3. The minimum total velocity increment obtained is 15.415 m/s, the shortest time of flight obtained is 2760 s, and the minimum combined dispersion is 0.800.

The trajectory of the minimum velocity increment solution is shown in Fig. 4. It can be observed that the field-of-view requirements within each rendezvous phase are satisfied. The light condition of the minimum velocity increment solution is shown in Fig. 5, in which the orbital transfer time intervals of the different rendezvous phases are shown by horizontal line sections labeled "segment *i*". It can be seen that the sun-illumination requirements within different rendezvous phases are satisfied.

In summary, the results for the single-objective optimal solutions have demonstrated the effectiveness of the proposed optimization model for a multiphase rendezvous mission.

C. Three-Objective Pareto-Optimal Fronts

Using NSGA-II, the three-objective Pareto-optimal solutions were successfully obtained and are presented in Fig. 6. As shown in Fig. 6, the Pareto-optimal solutions found approach the extreme values given by the single-objective optimal solutions. This confirms the effectiveness of the multi-objective optimization process and validates the Pareto-optimal solutions.

When the time of flight is less than 4000 s, the tradeoff relationship between the time of flight and the total velocity increment as well as the relationship between the time of flight and the combined

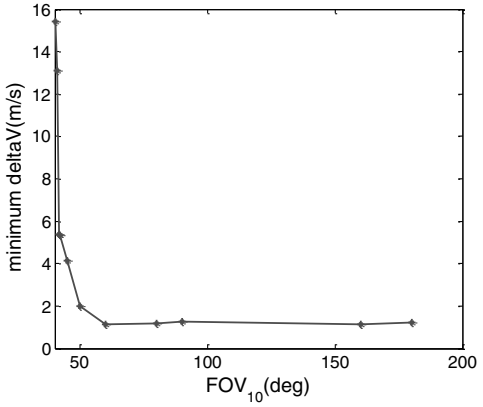

a) Minimum total velocity increment vs. field of view angle

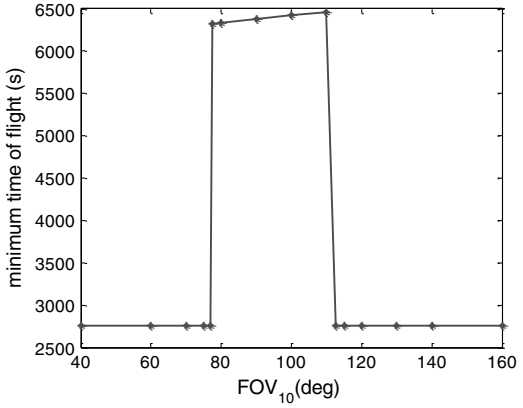

b) Minimum time of flight vs. field of view angle

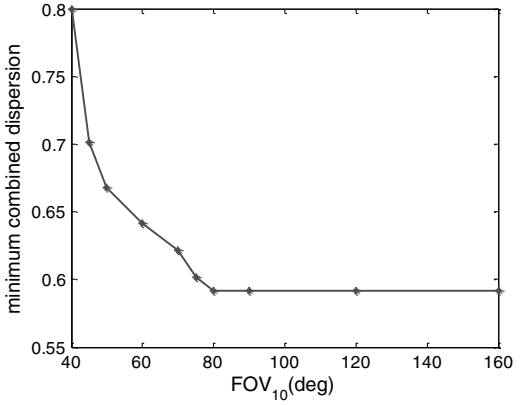

c) Minimum combined dispersion vs. field of view angle

Fig. 10 Relationships between field-of-view angle and different objectives.

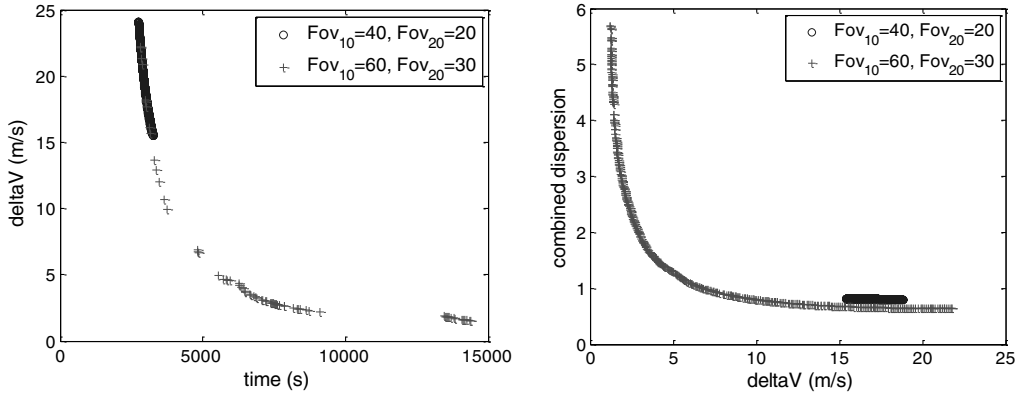

a) Total velocity increment vs. time of flight

b) Combined dispersion vs. total velocity increment

Fig. 11 Two-objective Pareto-optimal fronts comparison between different field-of-view angles.

dispersion are obvious. A longer time of flight would result in a lower total velocity increment and vice versa. Also, a longer time of flight would result in less combined dispersion and vice versa. However, when the time of flight is longer than 4000 s, the relationships between objectives are no longer obvious.

D. Two-Objective Fronts Comparison

The characteristics obtained from the three-objective Pareto-optimal fronts are a little unclear. To analyze the relationships between objectives more clearly, three comparisons of two-objective optimization results are made for three-, four-, and five-phase missions. They are presented in Figs. 7–9. Figure 7 shows the time of flight against total velocity increment fronts; Fig. 8 shows the time of flight against combined dispersion fronts; and Fig. 9 shows the total velocity increment against combined dispersion fronts.

From Fig. 7, it can be concluded that increasing the time of flight can effectively reduce the total velocity increment. Also, a three-phase mission is preferred from the point of view of the time of flight, while a five-phase mission is preferred from the point of view of the total velocity increment.

From Fig. 8, it can be concluded that the tradeoff relationship between the time of flight and the combined dispersion is weak. As in the three-objective case, a tradeoff is evident for the three-phase mission, but for the four- and five-phase missions, the Pareto-fronts are sparsely populated. In the four-phase and five-phase cases the Pareto-optimal points are tightly clustered, which indicates that the two objectives are in harmony rather than in conflict, and the combined dispersion cannot be reduced significantly by extending the time of flight.

From Fig. 9, it can be concluded that there is a clear tradeoff relationship between the total velocity increment and the combined dispersion. It is impossible to reduce the total velocity increment and the combined dispersion simultaneously even by changing the number of phases, and some compromise must be made between the two objectives during mission design.

E. Property Analysis

In this analysis, there are three phases, and FOV_{10} is changed while maintaining the relationship $\mathrm{FOV}_{20} = \mathrm{FOV}_{10}/2$. The minimum total velocity increment, the shortest time of flight, and the minimum combined dispersion obtained by the simple GA for different values of FOV_{10} are reported in Fig. 10. It is found that increasing the sensors' field-of-view angle appropriately can reduce the minimum total velocity increment and the minimum combined dispersion. However, this parameter has almost no impact on the shortest time of flight, except over a range of values where it makes matters decidedly worse.

To validate these observations, the two-objective Pareto-optimal fronts for the $\mathrm{FOV}_{10} = 40$ deg $/\mathrm{FOV}_{20} = 20$ deg and $\mathrm{FOV}_{10} = 60$ deg $/\mathrm{FOV}_{20} = 30$ deg cases are provided in Fig. 11. It can be seen that increasing the sensors' field-of-view angles appropriately can definitely improve the Pareto-optimal fronts for the total velocity increment and the combined dispersion, but it cannot reduce the time of flight significantly.

V. Conclusions

A multi-objective optimization approach has been proposed for multiphase orbital rendezvous missions and validated by application to a representative numerical problem. The results show that the proposed multiphase multi-objective orbital rendezvous mission optimization method is effective, and Pareto-optimal solutions satisfying engineering constraints are successfully obtained. By comparing the Pareto fronts obtained using the proposed method, the relationships between the three objectives considered are revealed, and the influences of other mission parameters, such as the sensors' field of view, can also be analyzed effectively.

Ultimately, the choice between Pareto-optimal solutions must be made by the designer/engineer using his/her experience and judgment or a formal multicriteria decision-making process. The benefit of the multi-objective approach advocated here is that the decision-maker is presented with a clear picture of what is possible and the tradeoff relations between the objectives before making that choice.

For multiphase orbital rendezvous missions, the tradeoff relationships between the total velocity increment and the trajectory robustness index as well as between the total velocity increment and the time of flight are obvious and clear. However, the tradeoff relationship between the time of flight and the trajectory robustness index is weak, especially for the four- and five-phase missions examined. Increasing the sensors' field-of-view angles appropriately can reduce the total velocity increment and improve trajectory robustness at the same time, but it cannot reduce the time of flight significantly.

The proposed approach could be used to reorganize a stable rendezvous profile for an engineering rendezvous mission, when there is a failure that prevents the completion of the nominal mission.

Acknowledgments

This work was supported by the National Natural Science Foundation of China (11222215), the Foundation for the Author of National Excellent Doctoral Dissertation (No. 201171) and the Science Project of the National University of Defense Technology (No. CJ12-01-02).

References

[1] Goodman, J. L., "History of Space Shuttle Rendezvous and Proximity Operations," *Journal of Spacecraft and Rockets*, Vol. 43, No. 5, 2006, pp. 944–959. doi:10.2514/1.19653

[2] Fehse, W., *Automated Rendezvous and Docking of Spacecraft*, Cambridge Univ. Press, London, 2003, pp. 31–32, 40–41, 113–170.

[3] Jezewski, D. J., Brazzel, J. P., Prust, E. E., Brown, B. G., Mulder, T. A., and Wissinger, D. B., "A Survey of Rendezvous Trajectory Planning," *Advances in the Astronautical Sciences*, Vol. 76, 1992, pp. 1373–1396.

[4] Won, C. H., "Fuel- or Time-Optimal Transfers Between Coplanar, Coaxial Ellipses Using Lambert's Theorem," *Journal of Guidance, Control, and Dynamics*, Vol. 22, No. 4, 1999, pp. 536–542. doi:10.2514/2.4430

[5] Luo, Y. Z., Liang, L. B., Wang, H., and Tang, G. J., "Quantitative Performance for Spacecraft Rendezvous Trajectory Safety," *Journal of Guidance, Control, and Dynamics*, Vol. 34, No. 4, 2011, pp. 383–389. doi:10.2514/1.52041

[6] Tang, G. J., Luo, Y. Z., and Li, H. Y., "Robust Optimal Linearized Impulse Rendezvous," *Aerospace Science and Technology*, Vol. 11, Nos. 7–8, 2007, pp. 563–569. doi:10.1016/j.ast.2007.04.001

[7] Breger, L., and How, J. P., "Safe Trajectories for Autonomous Rendezvous of Spacecraft," *Journal of Guidance, Control, and Dynamics*, Vol. 31, No. 5, 2008, pp. 1478–1489. doi:10.2514/1.29590

[8] Roger, A. B., and McInnes, C. R., "Safety Constrained Free-Flyer Path Planning at the International Space Station," *Journal of Guidance, Control, and Dynamics*, Vol. 23, No. 6, 2000, pp. 971–979. doi:10.2514/2.4656

[9] Zhang, J., Tang, G. J., Luo, Y. Z., and Li, H. Y., "Orbital Rendezvous Mission Planning Using Mixed Integer Nonlinear Programming," *Acta Astronautica*, Vol. 68, Nos. 7–8, 2011, pp. 1070–1078. doi:10.1016/j.actaastro.2010.09.024

[10] Dachwald, B., Seboldt, W., and Richter, L., "Multiple Rendezvous and Sample Return Missions to Near-Earth Objects Using Solar Sailcraft," *Acta Astronautica*, Vol. 59, Nos. 8–11, 2006, pp. 768–776. doi:10.1016/j.actaastro.2005.07.061

[11] Garner, C. E., Rayman, M. D., Brophy, J. R., and Mikes, S. C., "In-Flight Operation of the Dawn Ion Propulsion System Through Orbit Capture at Vesta," *47th AIAA/ASME/SAE/ASEE Joint Propulsion Conference and Exhibit*, AIAA Paper 2011-5661, 2011.

[12] Luo, Y. Z., Tang, G. J., and Lei, Y. J., "Optimal Multi-Objective Linearized Rendezvous," *Journal of Guidance, Control, and Dynamics*, Vol. 30, No. 2, 2007, pp. 383–389. doi:10.2514/1.21433

[13] Luo, Y. Z., Lei, Y. J., and Tang, G. J., "Optimal Multi-Objective Nonlinear Rendezvous," *Journal of Guidance, Control, and Dynamics*, Vol. 30, No. 4, 2007, pp. 994–1002. doi:10.2514/1.27910

[14] Luo, Y. Z., Tang, G. J., and Parks, G., "Multi-Objective Optimization of Perturbed Impulsive Rendezvous Trajectories Using Physical Programming," *Journal of Guidance, Control, and Dynamics*, Vol. 31, No. 6, 2008, pp. 1829–1832. doi:10.2514/1.35409

[15] Vasile, M., and Zuiani, F., "Multi-Agent Collaborative Search: An Agent-Based Memetic Multi-Objective Optimization Algorithm Applied to Space Trajectory Design," *Proceedings of the Institution of Mechanical Engineers, Part G: Journal of Aerospace Engineering*, Vol. 225, No. 11, 2011, pp. 1211–1227. doi:10.1177/0954410011410274

[16] Geller, D. K., "Linear Covariance Techniques for Orbital Rendezvous Analysis and Autonomous Onboard Mission Planning," *Journal of Guidance, Control, and Dynamics*, Vol. 29, No. 6, 2006, pp. 1404–1414. doi:10.2514/1.19447

[17] Deb, K., *Multi-Objective Optimization Using Evolutionary Algorithms*, Wiley, Chichester, England, U.K., 2002, pp. 171–285.

[18] Srinivas, N., and Deb, K., "Multiobjective Function Optimization Using Nondominated Sorting Genetic Algorithms," *Evolutionary Computation*, Vol. 2, No. 3, 1995, pp. 221–248. doi:10.1162/evco.1994.2.3.221

[19] Deb, K., Pratap, A., Agarwal, S., and Meyarivan, T., "A Fast and Elitist Multi-Objective Genetic Algorithm: NSGA-II," *IEEE Transactions on Evolutionary Computation*, Vol. 6, No. 2, 2000, pp. 182–197. doi:10.1109/4235.996017

[20] Vallado, D. A., *Fundamentals of Astrodynamics and Applications*, 2nd ed., Microcosm, Torrance, CA, 2001, pp. 263–271.